Physical Modelling in Geotechnics

Investigation of anchor installation for floating offshore wind turbines

D.A. Dao, K. Dicke & J. Grabe
Institute of Geotechnical Engineering and Construction Management, Hamburg University of Technology, Germany

ABSTRACT: With offshore wind turbines being constructed in water depths greater than 40 m, floating offshore wind turbines (FOWT) become more cost-effective than conventionally founded alternatives. However, sea bed anchoring of such floating bodies is yet not well understood, and deeper insights into the anchor-soil-interaction are crucial for the operation safety of these structures. Installation effects of the anchor-soil-interaction are often ignored. In this scope of work, installing a drag embedment anchor (DEA) in sea soil is simulated and analyzed using FEM with the Coupled Euler-Lagrange approach. The soil state is examined before and after installation. Results show a major change in the soil state surrounding the anchor. The performed simulations are planned to be validated by centrifuge tests to derive macroelements that accurately represent the load response of FOWT anchors in sea soil. Discrepancies between simulation results and conventional calculations show that considerations regarding more complex soil models and installation effects must be included when designing FOWTs in order to improve the prediction of the platform movement and ensure FOWT safety.

Keywords: anchor installation, FOWT, offshore geotechnics, drag embedment anchor (DEA), CEL

1 MOTIVATION

Anchors as anchoring points for offshore wind turbines (OWT) require less effort to install and to deconstruct than piles. Furthermore, ecology is less effected by not having to drive or to vibrate these foundations into the submarine soil (Ma et al., 2019). However, current research does not reflect a satisfactory understanding of soil-anchor interaction. There are analytical approaches (Aubeny and Chi, 2010; Neubecker and Randolph, 1996) to approximate the trajectory and capacity of a drag embedment anchor (DEA). Still, the embedment process of the anchor in the seabed and its effect on the bearing behavior is rarely considered. Therefore, a series of numerical simulations and experimental tests are planned to gain further insights into anchor-soil-interaction. This scope of work presents the first steps of developing a numerical model intended to be validated against centrifuge tests.

2 DRAG EMBEDMENT ANCHORS (DEAS)

Dimensions of DEAs depend on their weight, and moreover, their height depends on the shaft angle. The DEA consists of two main components, the shaft, and the flukes, of which the angle between these two distinguishes between soft clay and sand. For sand, the shaft angle is usually set at about 30 °, while for soft clays, the angle is set at 50 °. Depending on the soil properties and the shaft angle, the required drag distance for installation is longer for soft clays and shorter for sands. The installation of a DEA is done with the support of anchor handling vessels (Vryhof, 2015).

3 MODELING OF ANCHOR INSTALLATION

A simplified 3D anchor model has been developed based on a given CAD model of a Stevshark anchor from manufacturer Vryhof. In order to model the installation process, a soil body is needed corresponding to the distance and depth of the embedment process. Existing symmetries are exploited to reduce computational time.

3.1 Coupled Eulerian-Lagrangian method

The coupled Eulerian–Lagrangian (CEL) approach available in Abaqus/Explicit 2020 is used. In the Eulerian region, the Eulerian Volume Fraction EVF ($0 \leq EVF \leq 1$) describes the motion of material through the fixed mesh, indicating to which degree a Eulerian element is filled with material. Abaqus/Explicit uses a general contact algorithm with hard contact based on a penalty method. This method allows the Lagrangian elements to move freely through the Eulerian region until crossing an element filled with material ($EVF \neq 0$). Only then contact is established. In this work, an explicit time integration procedure is applied, which allows the solution of the next time step to be determined directly from the previous time step so that no iteration is needed. (Dassault Systèmes, 2021; Qiu, Henke and Grabe 2011) This method has been proven in various offshore applications (Osthoff, Heins and Grabe, 2017; Stapelfeldt et al., 2020; Bienen et al., 2021).

3.2 Numerical model of the anchor

Figure 1 presents different views of the simplified

© 2022 KOREAN GEOTECHNICAL SOCIETY (KGS), Seoul, Korea, ISBN 978-89-952197-7-5

anchor model. Figure 2a shows the reduced model with angles 32 ° and 50 °. Figure 2b and 2c show an overlay of the original model with the simplified model featured by red edge lines for both angle settings. For this work, a Stevshark model with a weight of 20 t with 7.3 m in length and 6.8 m in width is considered.

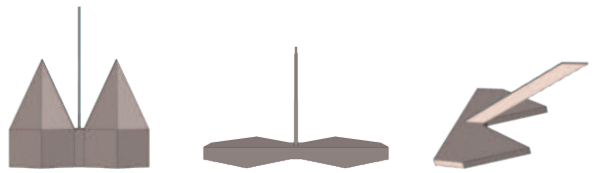

(a) (b) (c)

Fig. 1. Simplified anchor model with a shaft angle of 32 °: bottom view (a), rear view (b), three-dimensional view (c).

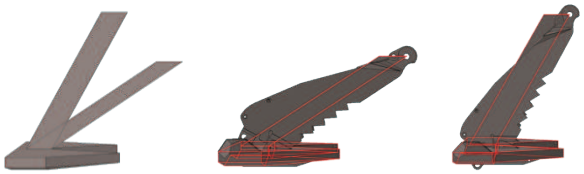

(a) (b) (c)

Fig. 2: Simplified anchor models (a), overlay of the original model with the simplified model for 32 ° (b) and 50 ° (c).

The steel anchor is modeled as a rigid body due to its significantly higher stiffness compared to the soil. Therefore, the center of mass and moments of inertia are read from the original model and assigned to the simplified anchor model.

3.3 Numerical model of the soil domain

Since the DEA's drag distance and penetration depth vary greatly depending on the soil and recommended shaft angle, two soil models are created: sand for a shaft angle of 32 ° and clay for a shaft angle of 50 °. For a 20 t Stevshark anchor, the values listed in Table 1 are obtained according to the manufacturer, which are used to determine the dimensions of the soil model.

Table 1: Penetration depth and drag distance for different soils of the Stevshark anchor according to Vryhof (2015).

Soil	Shaft angle [°]	Penetration depth d [m]	Drag distance [m]
Soft clay	50	19.0	97.5
Sand	32	6.0	36.0

Distances between the edges and the anchor depend on the anchor geometry h, l and w and the expected penetration depth d, as shown in Fig. 4. The effective anchor width w is 3.31 m resulting in a soil model width of 10 m. Here, only half of the anchor width is included due to symmetry. The maximum length l is 7.3 m. The maximum anchor height h is 4.2 m. The resulting dimensions of the soil bodies are shown in Table 2.

Table 2: Dimensions of the soil models.

Soil	Length [m]	Width [m]	Depth [m]	Void [m]	Elements
Soft clay	126.7	10.0	38.0	8.4	1 233 225
Sand	65.2	10.0	12.0	8.4	273 750

For the material behavior, linear elasticity with the boundary condition according to Mohr-Coulomb is applied. Table 3 lists the applied parameters of the soils determined by laboratory tests.

Table 3: Soil parameters.

Soil	Clay	Sand
Density ρ [t/m^3]	1.7	1.9
Young's Modulus E [kPa]	4 740	16 000
Poisson's ratio ν [-]	0.2	0.3
Friction angle φ [°]	22.98	33.58
Dilatation angle ψ [°]	0.01	0.21
Cohesion c [kPa]	0.20	0.01

Figure 3 shows the generated mesh of the anchor and the soil domain and Fig. 4 and 5 present the mesh for the soil domains.

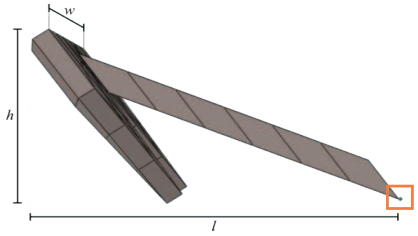

Fig. 3: Meshed DEA with additional cuboid marked in red.

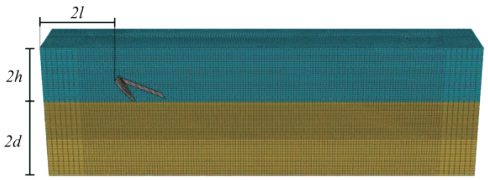

Fig. 4: Launch arrangement of the DEA with a shaft angle of 32 °.

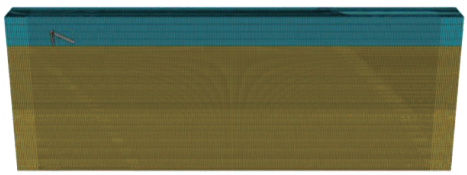

Fig. 5: Launch arrangement of the DEA with a shaft angle of 50 °.

3.4 Load history and boundary conditions

The anchor drops from a height of 0.50 m before the dragging process begins. Figure 5 shows the launch arrangement. During the installation process, the anchor is dragged in x direction after settling and also moves towards the z direction due to embedment. Horizontal forces perpendicular to the dragging in positive x direction on the anchor are not expected due to its simple mirror symmetry. In the case of the soil, the existing

symmetry is exploited, and only one-half of the width is considered. The simulation runs in two steps. Table 4 gives an overview of the conducted steps.

Table 4: Simulation steps.

Step	Process	Load	Duration [s]
0	Initialization	Predefined fields, boundary conditions	-
1	Gravity	Gravity	15.0 s
2	Dragging	Tension	36.0 s (sand) 97.5 s (clay)

First, gravity acts on the system for one second, then the dragging process begins. The boundary conditions are implemented into the model via displacement and rotation boundary conditions. The soil is allowed to move generally freely. At the edges, soil translation perpendicular to the *z*-*x* surface is inhibited. The anchor is allowed to move in *x* and *z* direction, as well as to rotate about the *y*-axis. Due to the rigid definition of the anchor model, all influences on it are controlled by a reference point located at the center of mass. Therefore, the dragging force cannot act directly on the shaft itself. Since a dragging force at the center of mass does not lead to realistic results, a cuboid functioning as pulling body is created that is connected to the shaft tip via a coupling function, see Fig. 3. The distance of the pulling body to the anchor shaft is fixed. The dragging process is implemented in the simplified model in a displacement-controlled manner. In Step 2, velocity *v* of 1 m/s acts on the pulling body, which transmits the velocity to the anchor. The duration of Step 2 depends on the drag distance.

4 RESULTS OF CEL ANALYSIS

For the output, the stresses in the soil, the embedment depth, and the drag distance are calculated. These values are generated for the expected lowest point, the lower anchor fluke tip.

4.1 Anchor Penetration Depths

Figure 6 shows the penetration depths vs. drag distance for both DEAs with a shaft angle of 32 ° and 50 ° into their respective soil. The drag velocity is 1.0 m/s for both simulations. For the sand, the drag distance is 36.0 m. The simulated maximum anchor penetration depth in the sand is 3.2 m being below the expected depth of 6.0 m, according to the manufacturer in Table 1. The drag distance for the DEA in clay is 97.5 m. The anchor penetration depth of 19.0 m according to the manufacturer is not reached in the simulation with soft clay. Here, the maximum depth is 6 m. Overall, the curve for the penetration process in the sand approaches one value, while the penetration in the soft clay continues to decrease. In both curves, the anchor rises slightly after a maximum depth towards the end of the simulation.

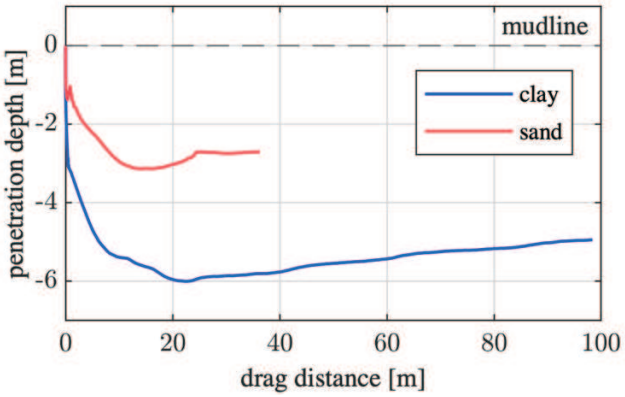

Fig. 6: Comparison of anchor penetration depths in sand and soft clay over the drag distance in Step 2.

4.2 Stress distribution in the soil

Figures 7 and 8 show the initial position of the simulation and the completion of the embedding process of the DEA with a shaft angle of 32 ° in sand. The upheaval of the soil due to anchor penetration is observed in Fig. 8. The stresses are highest directly in front of the anchor flukes and the connection of the shaft to the anchor flukes. The embedment process exerts influence on the stress distribution, see Fig. 8.

Fig. 7: Qualitative horizontal stress distribution for the embedding process of the DEA in sand: initial situation.

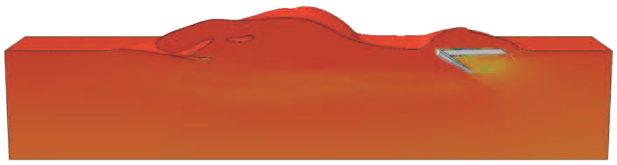

Fig. 8: Qualitative horizontal stress distribution for the embedding process of the DEA in sand: end of drag distance.

Figures 9 and 10 show the horizontal stresses in the soil at the initial position and the end of the embedment process of the DEA. The largest stresses are encountered in front of the anchor but are not clustered to local maxima compared to the embedment process in the sand.

© 2022 KOREAN GEOTECHNICAL SOCIETY (KGS), Seoul, Korea, ISBN 978-89-952197-7-5

Fig. 9: Horizontal stress distribution for the embedding process of the DEA in soft clay: initial position.

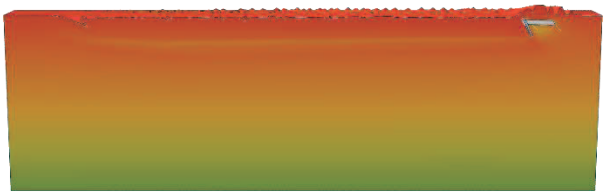

Fig. 10: Horizontal stress distribution for the embedding process of the DEA in soft clay: end of drag distance.

5 DISCUSSION

It is necessary to check if the required load-bearing capacity for the floating turbine is guaranteed by installing the DEA into the seabed. Table 5 lists the expected and simulated depths. Based on these values, a discrepancy is observed.

Table 5: Comparison of anchor penetration depths in sand and soft clay between the expected values according to Vryhof (2015) and the simulated results.

Soil	Sand	Soft clay
Expected penetration depth	6.0 m	19.0 m
Simulated penetration depth	3.2 m	4.5 m

Higher-order constitutive models for hypoplasticity by von Wolffersdorff (1996) and visco-hypoplasitcity by Niemunis (2003) are recommended for subsequent models to reproduce the complex relationships between stress and strain of soils in more detail. The simplified model might have to be extended in order to be able to reproduce the embedding process into different soils more accurately. For a realistic soil response to the dragging process, a force-controlled anchor dragging in Step 2 is essential, while following instructions of the manufacturers on the installation process.

6 SUMMARY AND OUTLOOK

Numerical investigations are an essential tool for understanding anchor-soil interaction. The foundation to develop a numerical model to simulate the installation process of anchors of FOWTs has been laid in this work. A simplified Stevshark anchor model has been created. The numerical simulation generally represents the installation process and shows its possible effect on soil stress state, but the results do not align with expected penetrations depths from manufacturers. To more accurately replicate the embedment process, suggested optimizations are recommended. Essential for accurately predicting soil behavior is implementing a hypoplastic constitutive model to reproduce the soil reactions due to anchor behavior and eventually validating results by, e.g., *ng*-tests in centrifuges. Validated numerical modeling and simulation of anchors of FOWTs are promising to allow for a better understanding of embedment behavior and its possible effect on a DEA's load-bearing behavior.

ACKNOWLEDGEMENTS

We thank Vryhof for providing us a CAD model of their Stevshark anchor.

REFERENCES

Aubeny C. P. and Chi C. 2010. Mechanics of Drag Embedment Anchors in a Soft Seabed. Journal of Geotechnical and Geoenvironmental Engineering 136 (1), 57-68.

Bienen B., Fan S., Schröder M. and Randolph M. F. 2021. Effect of the Installation Process on Monopile Lateral Response. Proceedings of the Institution of Civil Engineers - Geotechnical Engineering 174 (5), 530-548.

Dassault Systèmes. 2021. Abaqus documentation.

Ma K.-T., Luo Y., Kwan C.-T. T., and Wu Y. (1st) 2019. Mooring system engineering for offshore structures. Gulf Professional Publishing.

Neubecker S. R. and Randolph M. F. 1996. The Performance of Drag Anchor and Chain Systems in Cohesive Soil. Marine Georesources & Geotechnology 14 (2), 77-96.

Niemunis A. 2003. Extended hypoplastic models for soils. Ruhr-Universität Bochum: Chair of Soil Mechanics, Foundation Engineering and Environmental Geotechnics.

Osthoff D, Heins E. and Grabe J. 2017. Impact on submarine cables due to ship anchor - soil interaction. geotechnik 40 (4), 265-270.

Qiu G., Henke S., Grabe J. 2011 Application of a Coupled Eulerian–Lagrangian approach on geomechanical problems involving large deformations. Computers and Geotechnics. 38, 30-39.

Stapelfeldt M., Alkateeb D., Grabe J. and Bienen B. 2020. Numerical Simulation of Cone Penetration Tests Inside Suction Caisson Foundations in Sand. Offshore Geotechnics 10. American Society of Mechanical Engineers

Vryhof (5th) 2015. Anchor Manual - The Guide to Anchoring.

von Wolffersdorff P.-A. 1996. A hypoplastic relation for granular materials with a predefined limit state surface. Mechanics of Cohesive-Frictional Materials 1, 251-271.